Lamellar Diblock Copolymer Grain Boundary Morphology. 2. Scherk Twist Boundary Energy Calculations

Samuel P. Gido† and Edwin L. Thomas*

Department of Materials Science and Engineering, Program in Polymer Science and Technology, Massachusetts Institute of Technology, Cambridge, Massachusetts 02139

Received May 6, 1993; Revised Manuscript Received November 8, 1993®

ABSTRACT: The Scherk surface morphology allows a diblock copolymer lamellar phase to maintain microphase separation across a twist grain boundary. The interface between the two microphases in the Scherk grain boundary approximates a minimal surface consisting of a doubly periodic array of saddle surfaces. Grain boundary energies were calculated for the Scherk surface morphology as a function of diblock chain characteristics and as a function of grain boundary twist angle. The basic approach to grain boundary energy calculation is to formulate a general expression for the local free energy density as a function of chain characteristics and of the local curvature of the interface. The local energy density is then integrated over the mathematical model for the Scherk grain boundary. Two general methods of calculation were used, and the results were then compared. First, a self-consistent-field (SCF) model was formulated in which average energies per chain were calculated for all the possible interfacial curvature environments encountered by diblocks in the Scherk morphology. A second approach utilized a continuum (Helfrich) model for interfacial deformation in which moduli are used to impose energetic penalties for curvature of the interface in the grain boundary region. The application of this approach to block copolymers was provided by the model of Wang and Safran. The Wang and Safran model yielded results which agreed quite closely with those found using the SCF calculation.

I. Introduction

Diblock copolymer materials which form microphase-separated morphologies such as spheres, cylinders, ordered bicontinuous double diamond (OBDD) and lamellae also form larger scale grain structures. The specific structure of the grain boundary regions between grains has a great impact on material properties, such as the elastic modulus and gas permeability, that depend on the continuity of the individual phases across the grain boundaries. This paper is the second in a series of four on the grain boundary morphology of lamellar diblock copolymers designated GB-I,[1] GB-II, GB-III,[2] and GB-IV.[2] Here we present grain boundary energy calculations for Scherk's first surface[3] twist boundary morphology observed with transmission electron microscopy (TEM) in GB-I. In GB-I we discussed some general features of the grain structures of lamella-forming poly(styrene-*b*-butadiene), SB, diblock copolymers. Then we characterized two specific twist grain boundary morphologies: the helicoid section, observed at low twist angles, and Scherk's first surface, observed over the full range of twist angles from 0° to 90°. Figure 1 shows the mathematical interfacial geometry of the Scherk model for a 90° twist boundary.

Many researchers have developed models for the calculation of energies of block copolymers which are strongly microphase segregated into simple, commonly observed geometries such as spheres, cylinders, and lamellar sheets and more recently OBDD and lamellar catenoid morphologies.[4–15] These models are specific to particular microdomain geometries and cannot be directly applied to more complicated intermaterial dividing surfaces (IMDS) such as Scherk surface saddle regions or helicoid sections. (As in GB-I, the intermaterial dividing surfaces in the grain boundary regions, and in other defect structures, have been designated IMDS† to distinguish them from the interfacial surfaces in equilibrium microdomain morphologies which are designated IMDS.) What is required for our purposes is a method for calculating the free energy density at any point on an arbitrarily curved diblock interface as a function of polymer chain characteristics and of the local geometry of the IMDS† at the point of interest. Such an expression can then be integrated over the IMDS† in the grain boundary region of assumed model geometry, in order to calculate grain boundary energies. Theoretical results of Wang and Safran,[16–18] which are relevant to this problem of calculating diblock energies for interfacial surfaces of arbitrary,

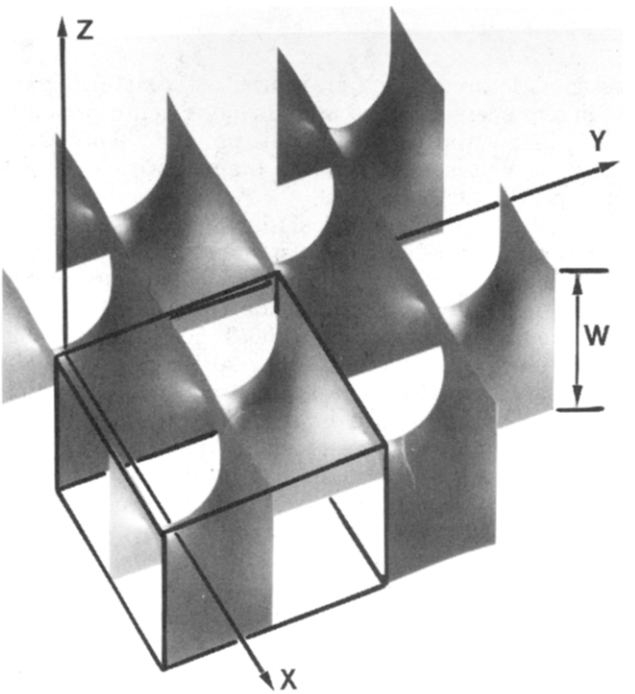

Figure 1. Intermaterial dividing surface of the 90° Scherk twist boundary morphology. The boldly boxed region containing two saddle surfaces is the unit cell of the structure. The grain boundary width, *W*, is also indicated.

* To whom correspondence should be addressed.
† Present address: Department of Polymer Science and Engineering, University of Massachusetts, Amherst, MA 01003.
® Abstract published in *Advance ACS Abstracts,* January 1, 1994.

0024-9297/94/2227-0849$04.50/0

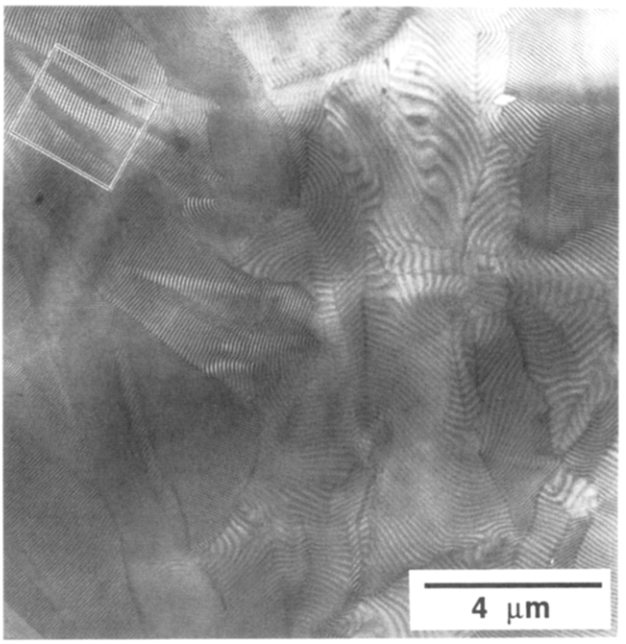

Figure 2. TEM micrograph showing the grain structure in a lamella-forming diblock copolymer: SB 80/80. The left half of the micrograph displays a kink-banded structure, while the right half shows an equiaxed grain structure more likely to have resulted from a nucleation and growth process. The boxed region contains a particularly good example of the kink band structure.

but small, local curvature, are utilized to estimate the grain boundary energies. Also more involved self-consistent-field models were applied to this problem. This study allows comparison of results obtained with different calculational methods.

We will present energy calculations for both the helicoid section and Scherk surface twist boundary morphologies as a function of twist angle. These grain boundary energy calculations are carried out for three different SB diblocks: molecular weights 20 500/20 500, 42 300/45 400, and 81 000/74 400 (designated SB 20/20, 40/40, and 80/80). These are the same symmetric, lamella-forming diblocks that were used in the TEM grain boundary characterization work presented in GB-I.

Finally, the methods described in this paper for the calculation of Scherk twist grain boundary energies will also be applied to the helicoid twist boundary in GB-III. In GB-IV tilt grain boundaries are analyzed.

II. Grain Structure Formation

Currently there has been no experimental or theoretical elucidation of the processes by which grain boundaries are formed in diblock copolymers. The experimental techniques of the present study, mainly direct imaging of fully formed grain boundaries via TEM, only allow us to speculate on the mechanisms that formed these structures. However, it will be helpful, as we endeavor to explain the observed morphologies through grain boundary energy calculations, to develop some ideas regarding possible processes of grain boundary formation. We begin by observing the grain texture in relatively low magnification images such as Figure 2 and GB-I Figure 1. TEM micrographs such as these suggest three possible mechanisms for grain boundary formation: (1) first-order nucleation and growth processes similar to that leading to the grain structures in metals and ceramics, (2) the superposition of stress fields around disclinations in focal conic textures typical of smectic liquid crystals, and (3) mechanically induced kinking or buckling of the lamella.

Some areas in the micrographs such as GB-I Figure 1 and the right part of Figure 2 exhibit grain structures somewhat reminiscent of metals. Fredrickson and Binder[19] have shown the microphase-separation process for lamellar diblock copolymers to be a fluctuation-induced, first-order phase transition. Microphase separation begins with composition fluctuations "nucleating", either heterogeneously or homogeneously, throughout the initially homogeneous copolymer material. Compositional waves coarsen and spread outward from these initial points. Fredrickson and Binder have analyzed this as a standard nucleation and growth process. Upon impingement, a collection of grains are formed. These grains are shaped like Voronoï polyhedra[20–22] and are separated by grain boundaries. The theory formulated by Fredrickson and Binder pertains to microphase separation of a polymer melt. In our present study of grain boundary morphology, all samples were prepared by casting from a toluene solution. The general result of Fredrickson and Binder's analysis, the occurrence of a first-order transition, may still be valid after modifications are made to account for a lower effective χ due to solvent shielding.[23] However, the most convincing evidence for this is found in the direct observation of the grain structure itself.

The initial geometry of the grain boundary IMDS†, formed by the impingement process, may have a relatively high energy. However, the grain boundary should be able to relax to a lower energy structure. This relaxation process would likely involve rearrangements of surface geometry that lead to an overall reduction in the area of the IMDS† in the grain boundary region as well as a reduction in unfavorable polymer chain conformations.

It might be imagined that spreading the required reorientation of the lamella out over a wider boundary region could lead to a reduction in the free energy per unit volume of the diblock material in the grain boundary region due, for instance, to a reduction in the amount of interfacial curvature per unit volume. It will be shown later, however, that the Scherk surface twist boundary has a fixed effective width, W, as illustrated in Figure 1. W is a function of the twist misorientation and is always on the order of one lamellar long period.

As shown in Figure 3, reproduced from Bouligand[24] Figures 22 and 23, the superposition of stress fields in a focal conic texture can lead to grain boundary-like wall structures. Figure 3a shows that perfect focal conic structures cannot completely fill space. In the crevices between the focal conics, as shown in a two-dimensional section in Figure 3b, material is drawn in to fill space, creating chevron-like wall structures. In this case delocalization of the curvature, resulting in widening of the wall/boundary region, is unlikely since these structures are stabilized by the presence of the focal conic stress fields. However, the detailed geometry in the boundary region is the result of a competition between the stress field and the curvature elasticity of the lamellae. Stiffer lamellae form a more diffuse, lower curvature, wall for a given stress field than more flexible lamellae. This type of focal conic wall texture is evident in GB-I Figure 1, where walls or grain boundaries are observed radiating out from the cores of disclination line defects as in the schematic of Figure 3.

Finally, the left half of the micrograph in Figure 2 exhibits a third type of texture observed in lamellar diblocks. Here the "grains" form long strips with a common general orientation. The "grain boundaries" seem to form long approximately parallel ridges. The anisotropic nature of this texture rules out the nucleation and growth process

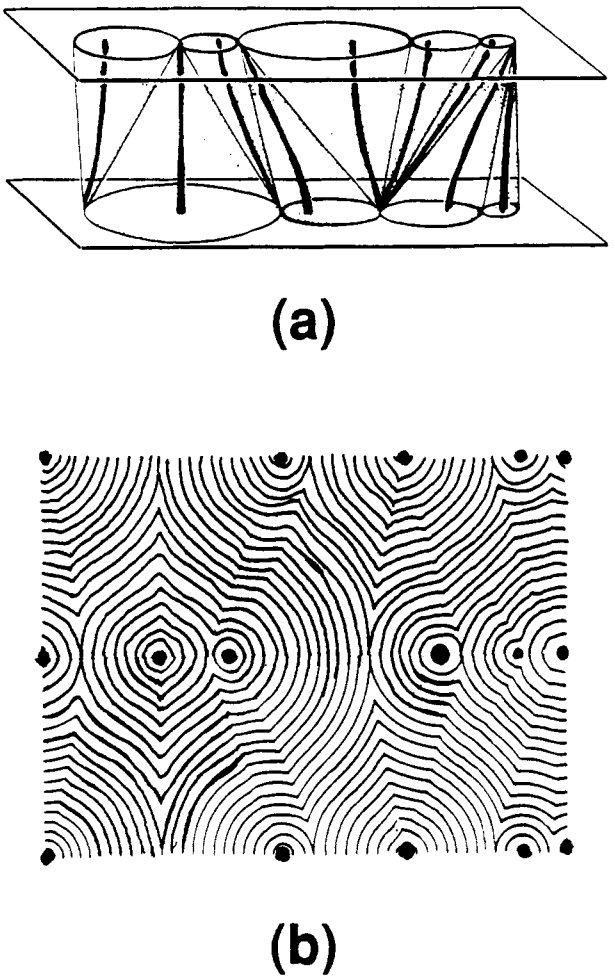

Figure 3. Grain boundaries as walls in focal conic textures. (a) A three-dimensional perspective view of an arrangement of disclination lines in a focal conic texture. The bold vertical lines represent the disclination cores, while the conic shapes represent the focal conic domains. (b) A schematic two-dimensional slice through this type of structure. Such a slice is similar to what is observed by TEM. The bold dots represent disclination cores. Walls or tilt grain boundaries result from the superposition of the disclination stress fields as material relaxes to fill the space between the focal conics. These walls appear to radiate outward from disclination cores. Reprinted with permission from ref 24. Copyright 1972 Journal de Physique.

which is expected to produce equiaxed grains. Instead this texture appears to be the result of mechanically induced kinking of the lamellar structure. This kinking results from a compression along the lamellar planes or a tension normal to the lamellae.[25,26] As opposed to the local stress fields due to focal conics, discussed in the previous paragraph, the stress producing these kinks was unidirectional and long ranged. A possible source of these stresses is uneven material shrinkage during the casting of the diblock films from solution. At some relatively late stage of the solvent removal process the lamellae will have already formed and lost enough of their mobility that further anisotropic shrinkage in the final stages of solvent removal will cause them to buckle. The analysis of kinking geometry is well developed for materials such as metals,[27] composite materials,[28,29] and fiber-forming rigid-rod polymers.[30-33] The boxed region in Figure 2 contains a particularly good example of this kinking geometry.

The kinking of the lamellar structure produces bands of tilt boundaries only. The normal stresses that produce the kinks lack the torque components that would be necessary to deform lamellae into twist boundaries. Some twist boundaries may be observed in this kink banded region, but they were likely formed before the kinking process occurred. Note that the lamellae must be properly oriented with respect to the stress field for buckling to occur. This explains why in Figure 2 the buckling is only observed in the left half of the micrograph where the lamellae are all aligned more or less vertically. The analysis of kink band structures will not be pursued further in this series of papers on grain boundaries.

III. Interfacial Energy Calculations

The global equilibrium structure of a sample of lamellar diblock copolymer would be a single, macroscopic, lamellar pseudocrystal. However, given that grains exist as a result of a complex superposition of all three boundary-forming mechanisms discussed above, it seems reasonable to assume that the material in the narrow grain boundary regions assumes a local equilibrium structure within the constraints imposed by the orientations of the adjoining bulk lamellar grains. This assumption is supported by the repeated observation of the same two twist boundary morphologies, Scherk and helicoid section, both of which represent logical choices for solutions to the constrained equilibrium problem due to their minimization of interfacial areas.[1] Thus, calculating the free energies of such grain boundary regions, we feel justified in using methods which assume the grain boundary morphologies are in equilibrium.

Grain boundary energy calculations were performed for the material in the grain boundary region on a per unit volume or per chain basis. Since the grain boundary regions are narrow, essentially two-dimensional surfaces when viewed on the length scale of the grain structure of the material, one can also consider the Scherk boundary energies on a per unit area, of the *plane*[1] of the grain boundary, basis. The *plane* of the Scherk boundary is the $X-Y$ plane in Figure 1. Note that the area of this plane is not the same as the area of the IMDS†; in fact the area of this plane is generally much less than the interfacial area.

An expression for the local free energy density at a point on the IMDS† as a function of the interaction of the polymer molecular architecture and local geometry is integrated over the mathematical interface model and then normalized by boundary area or the volume of the boundary region. The local geometry of the IMDS† is fully specified by the two principal curvatures which are the reciprocals of the two principal radii of curvature at that point:[34] $c_1 = 1/R_1$ and $c_2 = 1/R_2$. It is possible to have principal curvatures of opposite sign in cases where the surface curves in two opposite directions simultaneously, and thus the centers of curvature are on opposite sides of the surface. The average of the two principal curvatures is called the mean curvature, $H = (c_1 + c_2)/2$, while their product is the Gaussian curvature: $K = c_1c_2$. The interfacial geometries of interest in this paper, the Scherk surface and the helicoid, are both minimal surfaces; a specification that means $H = 0$. Minimal surfaces, excluding the special case of the plane, have c_1 and c_2 equal in magnitude but opposite in sign, and thus the Gaussian curvature is everywhere negative or zero.

Two approaches to the calculation of the effect of this IMDS† geometry on local diblock energy have been considered. One approach is to explicitly calculate the equilibrium diblock layer characteristics and free energy at every point (or a finite element mesh of points) on the intermaterial dividing surface using a self-consistent-field theory formulated for grafted polymer chains which are strongly stretched relative to their unperturbed dimensions

(henceforth referred to as "SCF").[10,35,36,58] The second approach is to work by analogy to the classical theory of elasticity of membranes and express the free energy of the diblock interface at each point in terms of energy penalties (expressed as moduli) for deviations from the preferred or natural interfacial curvature.[18] Flat planes are the preferred interfacial shape for lamella-forming, symmetric diblock copolymers.

The most general grain boundary energy calculations are carried out by solving the SCF model for the chain conformation distribution and local energy density at a point on the IMDS† as a function of the local values of H and K. This local energy density must then be integrated over the IMDS†. Using a piecewise linear approximation for the chain end distribution function, we are able to get numerical solutions to the SCF model for diblock melts as a function of arbitrary local curvature.[37] Since the Scherk surface is a minimal surface, the only geometrical parameter that changes from point to point on the surface is the Gaussian curvature K. We were able to calculate the total energy per chain vs K with the SCF model. Chain energy vs K was then fit by a relatively simple analytical function which was integrated over the Scherk IMDS† to give grain boundary energies.

If the deviations of a diblock layer from its preferred curvature can be modeled with a continuum elasticity theory, then a considerably simplified working expression for the free energy density on a diblock copolymer IMDS† can be obtained. This approach, valid for relatively small curvatures, is very well established in the analysis of liquid crystalline textures,[38] microemulsions,[39,40] and lipid bilayers.[39,41] When applied to smectic liquid crystals/lamellar diblocks,[16-18,38,41,42] this general approach leads to the following form of the free energy, f, in deformed lamellae.

$$f = f_0 + kH^2 + \bar{k}K \tag{1}$$

Equation 1 may be formulated to give energy per unit interfacial area as is common in its application to microemulsions. However, due to the variability in the area per diblock chain on the IMDS† with curvature, Wang and Safran (WS)[16-18] have formulated a model using an expression of the same form to give an energy per chain. The form of eq 1 shown here is for the particular case, relevant to our diblock copolymer lamellar systems, in which the natural or preferred curvature of the layers is zero (flat planes). More general expressions for cases of nonzero preferred curvature can be found in refs 16-18. In eq 1, f_0 is the free energy per unit area or per chain of the minimum energy flat diblock interface, while H and K characterize the deviations from the flat interface up to a second-order dependence on curvature. k is a constant known as the splay modulus since it represents the energy penalty for the splay deformation mode as defined by Frank.[38] $\bar{k}$ is the saddle-splay modulus. It represents the energy penalty for a general type of three-dimensional curvature defined by both Frank and Helfrich.[41] In general, this type of curvature, known as saddle-splay curvature, involves both splay and twist of the director field. The director in a diblock copolymer material is taken everywhere as the direction of the chain stretching, normal to the interface. In smectics, however, twist is absent[26,38,41,43,44] and the saddle-splay curvature reduces to K. The name saddle splay derives from saddle surfaces, such as our Scherk saddles, which display this type of curvature in its pure form (i.e., no simultaneous mean curvature).

WS present an approach for the calculation of the curvature moduli, k and $\bar{k}$, for diblock copolymers. Their approach builds on the SCF results of Milner, Witten, and Cates (MWC)[35] and the extension of this model to curved, grafted homopolymer layers by Milner and Witten.[45] WS construct a power series expansion, up to second order in curvature, for the free energy of the diblock layer. In this expansion chain conformational energies are calculated for the diblock chains using the SCF approach, but with a key difference to the previous work of Milner *et al.*[35] WS allow the area per junction on the IMDS† to vary and find a minimum by balancing against the chain stretching terms (under the constraint of constant chain volume). This procedure yields the following result for the variation of interfacial area per chain Σ with curvature for symmetric lamella-forming diblocks:

$$\Sigma = (\Sigma^*)\left[1 + H^2 - \frac{2}{15}K\right] \tag{2}$$

where Σ^* is the area per chain on the flat interface:

$$\Sigma^* = (\pi^2/12)^{1/2}N^{1/3}\gamma^{-1/3} \tag{3}$$

N is the degree of polymerization, and γ is the interfacial energy or tension. In eq 2, H and K must be made dimensionless with respect to the equilibrium thickness of a flat grafted brush, h^*, which is one-quarter of the lamellar long period, L. Henceforth, "K" is used to refer to the dimensionless Gaussian curvature: $K(h^*)^2$. Recall that K is negative for our minimal surface grain boundary models. Thus, curving the surface in either a mean curvature or Gaussian saddle bending mode increases the area per junction. Equation 2 would seem to indicate that a positive Gaussian curvature, such as that displayed by a spherical interface, would decrease the area per chain. However, unlike a negative Gaussian curvature, a positive Gaussian curvature is always accompanied by a positive mean curvature whose effect dominates in eq 2. For instance, for a sphere of radius R the resulting increase in area per chain is given by $\Sigma = (\Sigma^*)\{1 + (13/15)(h^*/R)^2\}$.

Before proceeding, it is necessary to more closely examine the applicability of WS's work to our grain boundary morphologies. The WS theory is strictly applicable only for an isolated diblock layer. It assumes that the only important energy contributions are interfacial and chain stretching energies for that single layer with no external constraints other than the curvature that the layer is assumed to possess. A little reflection reveals that our grain boundary morphologies impose additional geometric constraints that alter the SCF problem, leading to different results from WS. We will proceed to first quantify the difference between the Scherk grain boundary problem and the WS problem. The SCF solution for the Scherk problem in section VI will then be compared to approximate results obtained by applying the WS theory in section V.

Through conservation of volume the interfacial area per chain, Σ (given by eq 2 in the WS case), is directly linked to the height, h, of the grafted layer of diblock chains. Figure 4a shows a piece of diblock interface with a Scherk saddle geometry and a polymer chain confined to an imaginary volume element. The sides of this volume element are all normal to the IMDS† at their points of contact, and the total volume of the element is equal to the volume of a chain. This element has area Σ at the interface. The area of a two-dimensional slice through this volume element, normal to the surface, at a height z above the surface, is $\Sigma(z) = (1 + zc_1)(1 + zc_2)\Sigma = (1 + 2Hz + Kz^2)\Sigma$. The conservation of volume constraint for a

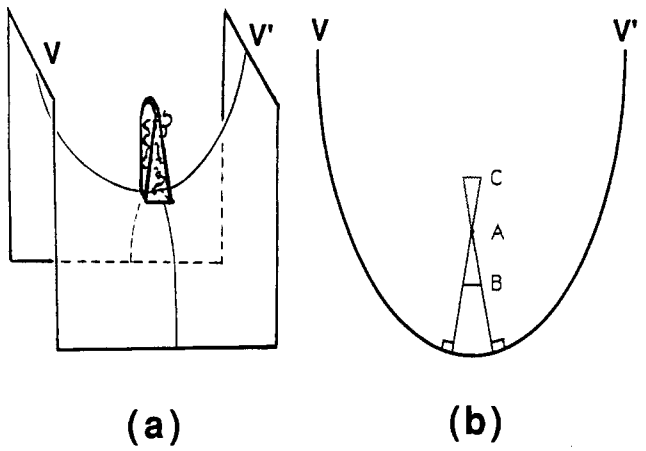

Figure 4. Space available to a diblock chain near a saddle-shaped interface. (a) A three-dimensional representation of the volume element occupied by one block of a diblock copolymer tethered to a saddle-shaped interface. (b) A two-dimensional slice through this structure along the curve VV'. The largest chain that can be accommodated near the interface fills this element to height A. Smaller chains fill the volume element to height B. Height C corresponds to an unphysical solution to the equation for brush height.

Table 1. Geometrical and Energetic Parameters for Lamella-Forming Diblock Copolymers

diblock	V_{pc} (nm^3)	Σ^* (nm^2)	f_0/kT	f_0^*/kT (nm^{-2})	$\bar{k}(h^*)^2/kT$	$\bar{k}^*/kT$
SB 20/20	74.7	3.86	6.9	1.8	−1.9	−46
SB 40/40	160	5.12	9.2	1.8	−2.41	−115
SB 80/80	315	5.95	10.5	1.8	−2.46	−290

single chain is[10]

$$\int_0^h \Sigma(z)\,dz = N_A\nu \tag{4}$$

where N_A is the degree of polymerization of the block on the side of the interface under consideration, and ν is the volume per monomer. Thus the product $N_A\nu$ is the volume of the A block. This integral may be performed to yield a cubic equation relating h and Σ:

$$\frac{1}{3}Kh^3 + Hh^2 + h - N_A\nu/\Sigma = 0 \tag{5}$$

Equations 4 and 5 are general conservation of volume results that relate Σ and h regardless of whether or not the WS result for Σ, eq 2, is valid.

We now examine the deviation of diblock layers in the Scherk surface geometry from the conditions of the WS theory. Our major tool is conservation of volume for incompressible polymer chains. Consider the Scherk surface unit cell shown in Figure 1. The volume of this unit cell is a function of twist: $V_u = WL^2/\sin\alpha$, where L is the long period, W is the grain boundary width, determined by criteria to be discussed in section IV, and α is the twist angle defined in GB-I Figure 2. The number of diblock chains in this unit cell, n, is given by V_u/V_{pc} where V_{pc} is the volume per chain. Values of V_{pc} and Σ^* for SB 20/20, 40/40, and 80/80 are given in Table 1. If we integrate chain junctions over the Scherk surface interface in this unit cell, we should get the same total number of chains:

$$n = \int\int_S dn = \int\int_S \frac{dA}{\Sigma} = \int\int_S \frac{|\mathbf{S}_u \times \mathbf{S}_v|\,du\,dv}{(\Sigma^*)(1 - bK)} \tag{6}$$

Here we have assumed the same functional form for Σ as the WS result. However, the coefficient of Gaussian curvature, b, is determined by solution of eq 6 for various twist values. Equation 6 is satisfied for twist values from 0° to 90° by $b = 0.5$, a value considerably greater than the WS result of 2/15. At the saddle points of the Scherk surface (exact center points of the saddles) the dimensionless Gaussian curvature, K, reaches its greatest magnitude of −2.47. This value occurs at the saddle points of all Scherk surfaces regardless of the twist angle. With $b = 0.5$ this curvature leads to an increase in Σ over Σ^* by a factor of 2.2 at the saddle points. Thus there is a large deviation from the WS result which predicts only a 30% increase in Σ at the saddle points. This indicates that the geometric constraints imposed on the diblock chains in the Scherk grain boundary region can significantly alter the problem from the conditions assumed in the WS theory. The full implications of these geometrical constraints are accounted for in the SCF calculations described in the next section.

IV. Self-Consistent-Field Calculation Results

The application of the SCF model to saddle-shaped interfaces in diblock melts is described in detail elsewhere.[37,60] The key to the solution of this problem is to determine a chain end distribution function $g(x')$ such that the conformational energy per chain

$$\Delta F_{el} = \frac{3}{2}\int_0^h g(x')\left\{\int_0^{x'} E(x,x')\,dx\right\} dx' \tag{7}$$

is minimized with respect to constraints such as conservation of volume and constant segmental density. Here x' denotes the position of the free end of a grafted chain. $E(x,x')$ is the local chain stretching energy at point x of a grafted chain with its free end at x'. Thus the inner integral represents the total chain stretching energy for a grafted chain with its end at x'. The outer integral then computes an average conformational energy per chain by summing over the brush height and weighting each energy by $g(x')$.

The brush height is a function of curvature, and Σ given by eq 5. The unique geometry of a saddle-shaped IMDS[†] leads to unusual results concerning h and Σ. As shown in Figure 4a the space available to a chain in the vicinity of a saddle surface is squeezed inward in one of the principal directions where the curvature is concave. This contraction of the available space, by itself, would necessitate increased chain stretching. The saddle IMDS[†] has another principal curvature, however, which is convex and allows the space available to a chain to increase in a direction orthogonal to the direction in which space is compressed. One might expect the contraction of space in the direction of the concave principal curvature and the expansion in the direction of the convex principal curvature to cancel out, leaving the amount of chain stretching approximately the same as for a flat grafting surface. This is, in fact, the case up to moderate Gaussian curvatures, but an additional complication arises at higher $|K|$.

Figure 4b shows the intersection of Figure 4a with a plane passing through the saddle point and containing the curve, VV', on the IMDS[†] of maximum (principal) concave curvature. The intersection of the chain volume element with this plane is also shown. Notice that the sides of the volume element are perpendicular to the IMDS[†] at their points of contact. The maximum size of the polymer chain that can be grafted to the surface with a given Σ is determined by the volume of this element when the sides of the element converge at point A. This represents the largest possible volume element for a given

K. Smaller chains may be grafted to the surface, and they fill the volume element up to some lower height B. Solution of eq 5 for h yields various types of results depending on K and Σ. For a fixed Σ, if the chain is small enough to be accommodated in the volume element, then the equation gives two real, positive roots for h. The smaller of these two roots gives the h value for the chain stretched to B. This is the physical solution. The larger root gives a height corresponding to C in the figure. In this case the artificial extension of the volume element beyond the convergence point, A, leads to the addition of "negative" volume to the element. Thus a second, unphysical root occurs when the negative volume between heights C and A exactly cancels the "positive" volume between A and B. As the chain approaches the maximum size that can be accommodated for a given combination of Σ and K, then the two roots for h converge to one value corresponding to point A. Finally, for chains larger than this maximum size no real positive roots exist for eq 5. In this case the chain cannot be accommodated unless Σ is allowed to increase.

If Σ were given by the WS result, eq 2, a symmetric diblock chain could fit onto a saddle-shaped IMDS† only up to a maximum $|K|$ of 0.506. For larger magnitudes of K the chain cannot be accommodated without increasing Σ. However, using the result previously determined for the Scherk geometry,

$$\Sigma(H=0,K) = (\Sigma^*)\{1 - 0.5K\} \quad (8)$$

we find that due to the increase in Σ, over the WS case, chains can be accommodated up to much higher $|K|$. For $|K| < 1$ the situation, illustrated by position B in Figure 4b, exists in which the volume element required is smaller than the maximum that is geometrically attainable. For $1 \le |K| \le 2.467$ the situation illustrated by position A exists in which the chain can just barely be accommodated by using the largest possible volume element. In fact, in the more highly curved regions of the saddle surface, it is important for brush height condition A to exist so as to completely fill the space above the IMDS† with polymer.

In the SCF model for the Scherk surface (SsSCF) the greater increase in Σ with increasing curvature results in a decrease in h/h^* down to a minimum value of 0.64 at the maximum $|K|$ value of 2.467. The decrease in brush height with increasing $|K|$ may be cause for concern since it could lead to a breakdown in the strong stretching assumption employed in the SCF model. We note, however, that the strong stretching assumption is valid[35,58] for $R_g \ll h \le h^*$. We show below that $h^* \sim N^{0.19}R_g$ ($R_g = N^{1/2}a/\sqrt{6}$). Since $h = O(1)\ h^*$ at $|K| = 2.47$, then $h/h^* \sim N^{0.19}$. Therefore, the strong stretching assumption should still be valid at $|K| = 2.47$ for large N. The limiting case for our experimental diblock systems is SB 20/20 in a $|K| = 2.47$ curvature environment. Here R_g, h, and h^* are 35, 62, and 97 Å, respectively. For SB 40/40 R_g, h, and h^* are 49, 100, and 156 Å; for SB 80/80 R_g, h, and h^* are 69, 170, and 265 Å. Thus the chains remain strongly stretched even at the highest possible Gaussian curvature, for all three diblocks considered.

Figure 5 shows the chain end distribution functions, $g(x')$, calculated with our numerical solution technique for various K values. These profiles, plotted vs the dimensionless length x'/h^*, are independent of molecular weight. Minimal surfaces, such as the Scherk surface, have the interesting property that the curvature environment is identical on both sides of the surface since the two principal curvatures are equal and opposite. In an A–B diblock, Figure 4a shows the volume element available to

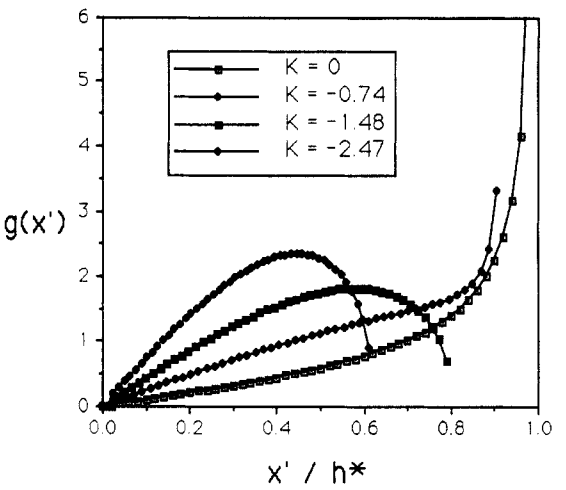

Figure 5. Chain end distribution functions $g(x')$ for various K values, ranging from 0 to −2.47, calculated by a numerical solution to the SCF model. This distribution function gives the relative concentration of free chain ends located at a fraction x'/h^* of the full brush height. These dimensionless plots are independent of molecular weight. At $K = 0$, the greatest concentration of chain ends is at or near the full brush height. With increasing $|K|$ the polymer brush height decreases and more chain ends become distributed throughout the brush height.

the A block on the upper side of the Scherk saddle. The volume element available to the B block on the lower side of the saddle has exactly the same shape but is rotated by 90° with respect to the element shown. Thus the $g(x')$ plots shown in Figure 5 are applicable for both blocks on both sides of the IMDS†. Although the grafted polymer brush gets shorter with increasing $|K|$ due to increasing Σ, the shapes of the $g(x')$ curves as $|K|$ increases follow a pattern of evolution somewhat similar to that found for brushes on the concave side of a cylinder.[36] The pattern displayed by both the cylindrically grafted chains and the chains on the Scherk interface involves a transition from a distribution where the chain ends are concentrated near the edge of the brush for the flat case to a situation where more of the chain ends are distributed throughout the brush as $|K|$ increases. On the concave side of a cylinder, as well as in the Scherk case, this change in chain end distribution with increasing curvature (H for the cylinder and K for the saddle) is a response to the decrease in available space to locate chain ends near the full brush height. This is evident, for instance, in Figure 4b.

Notice that there is no dead zone in these chain end distributions. Dead zones are regions of the brush from which chain ends are excluded. They generally manifest themselves as regions where $g(x')$ takes on unphysical, negative values. The presence of dead zones, which occur near the grafting surface for brushes grafted to strongly curved, convex cylindrical, or spherical surfaces, signals a breakdown of the parabolic chemical potential employed in the solution of the SCF model.[35,45,46,58] When these dead zones grow to a significant fraction of the brush height the validity of the analysis is jeopardized. The absence of dead zones in our results is encouraging.

Chain end distributions determined by the SsSCF analysis were then used in eq 7 to yield the average elastic energy per chain, F_{el}, as a function of K. The total energy per chain, F_{tot}, is equal to the sum of the elastic energy plus an interfacial energy term $F_{int} = \gamma\Sigma$, where γ is the interfacial energy or tension. In the SsSCF calculations we use $a = 6$ Å as a Kuhn length approximately applicable to both the PS and PB blocks. We take $\nu = 140$ Å^3 which is the average of the PS and PB volumes per monomer:

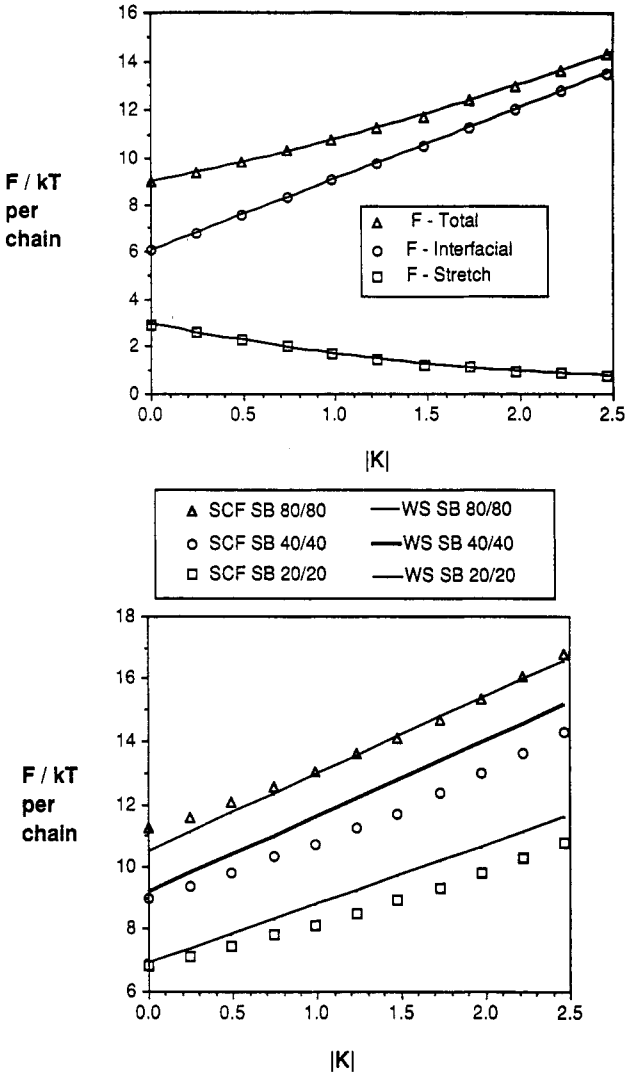

Figure 6. Energy per chain as a function of Gaussian curvature. (a) Plots of chain stretching and interfacial component energies as well as total energy per chain, calculated by a Scherk specific SCF model, for SB 40/40 as a function of $|K|$. The chain stretching energy decreases from 2.9 to 0.78 kT per chain as $|K|$ increases from 0 to 2.47. Over the same curvature range the interfacial energy per chain increases from 6.0 to 13.5 kT. This leads to an overall increase in the total energy per chain from 8.9 to 14.3 kT. The general trends displayed in this plot for SB 40/40 are also found in similar graphs for SB 20/20 and 80/80. (b) Total, average energy per chain, F_{tot}, vs $|K|$ for SB 20/20, 40/40, and 80/80. The symbols represent the results of the Scherk specific SCF model, while the lines were calculated using the WS approach. The total energy per chain increases with increasing Gaussian curvature for both calculation methods and for all three molecular weights.

180 and 100 Å^3, respectively. The interfacial energy, γ, was calculated from χ using the following relationship:[16,47] $\gamma = a\chi^{1/2}/v$. χ is a function of T and was calculated using the relationship[48] $\chi = -0.0937 + 66/T$, which gives a value of 0.074 at the annealing temperature of 120 °C (393 K). This gives a γ value at this temperature of 0.012 kT/Å^2.

Figure 6a shows the elastic energy, interfacial energy, and total energy per chain on the Scherk interface for SB 40/40 as a function of K. The results for the other two molecular weights are similar. Notice that, due to the decreasing brush height, the stretching energy per chain decreases from 2.9 to 0.78 kT as $|K|$ increases from 0 to 2.47. The following quadratic relationships, obtained by least-squares fitting, summarize the SCF results for chain conformational energy in SB 20/20, 40/40, and 80/80:

$$F_{el}(\text{SB } 20/20) = 2.25 - 1.08|K| + 0.168|K|^2 \quad (9a)$$

$$F_{el}(\text{SB } 40/40) = 2.94 - 1.49|K| + 0.250|K|^2 \quad (9b)$$

$$F_{el}(\text{SB } 80/80) = 4.21 - 1.93|K| + 0.267|K|^2 \quad (9c)$$

Over the same $|K|$ range, in SB 80/80, the interfacial energy per chain increases from 6.0 to 13.5 kT due to the increase in Σ. This leads to an increase in the total energy per chain with increasing $|K|$. Figure 6b shows the total energy per chain for the three different molecular weights. The symbols represent the SsSCF energies, while the lines give the results of the WS approach to be discussed in section V. Least-squares fitting of the SsSCF results gives the following quadratic relationships between total energy per chain F_{tot} and $|K|$ for the three different molecular weights:

$$F_{tot}(\text{SB } 20/20) = 6.80 + 1.19|K| + 0.167|K|^2 \quad (10a)$$

$$F_{tot}(\text{SB } 40/40) = 8.99 + 1.53|K| + 0.250|K|^2 \quad (10b)$$

$$F_{tot}(\text{SB } 80/80) = 11.2 + 1.59|K| + 0.265|K|^2 \quad (10c)$$

In eq 10 the constant terms correspond to f_o, the flat interface energy in the Helfrich expression, eq 1. The second terms in eq 10 correspond to the linear relationship between energy and K, also present in the Helfrich expression. Finally the terms in $|K|^2$ represent a second-order correction to the Helfrich expression. Note, however, that these Helfrich expressions with second-order corrections are not general but apply only to the specific case of the Scherk saddle morphology.

Comparing the numerical coefficients in eqs 9 and 10, it is evident that the $|K|^2$ dependence of the total energy per chain comes directly from the SCF conformational energy per chain. This is because in using eq 8 for Σ we have assumed only a linear dependence for the interfacial energy per chain on $|K|$. We will, however, retain these results since a linear variation of Σ with $|K|$ was sufficient for the solution of eq 6.

The results given above in eqs 9 and 10 allow the determination of the scaling relationship between energy per chain and N.

$$F_{el} \sim N^{0.46} \quad (11a)$$

$$F_{int} \sim N^{0.31} \quad (11b)$$

$$F_{tot} \sim N^{0.35} \quad (11c)$$

These relationships are independent of K. The scaling law for F_{tot} will be discussed further in section V where it will be compared to the predictions of WS. The scaling of the interfacial energy is easy to understand: $F_{int} \sim \Sigma = V_{pc}/L \sim N/N^{\nu} = N^{1-\nu}$, where ν is the scaling exponent relating lamellar long period to N. In the strong segregation limit ν is expected to equal $^2/_3$, but for the three block copolymers used in this study it was found by SAXS to be 0.69. At the annealing temperature of 120 °C, however, these three molecular weights span a range of χN from about 35 to 140. Thus our scaling exponent for L results from a combination of intermediate[59] and strong segregation results. The scaling law for chain stretching energy, eq 11a, may at first appear surprising since the conformational energy of grafted brushes is expected[35,46,49-51] to scale as N^1. However, this scaling law refers to the case where N is increased for a fixed area per chain on the grafting surface, Σ. In the present case the effect on F_{el} of increasing N is partially offset by an increase in Σ.

From eq 10, the free energy per chain at a point on the Scherk IMDS† is known as a function of the local curvature.

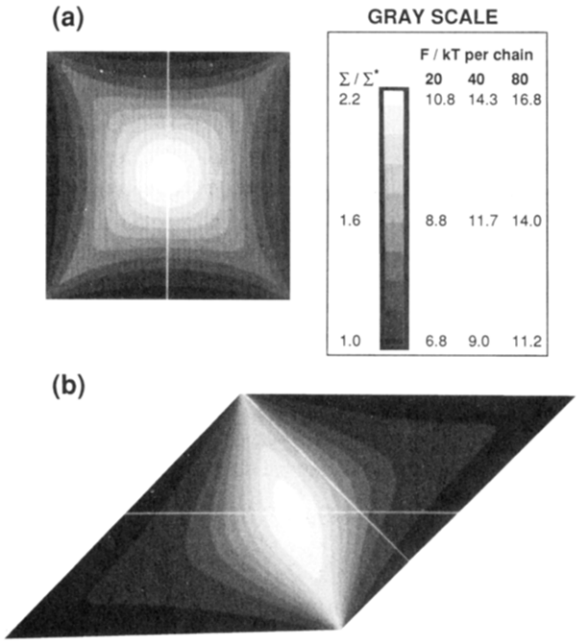

Figure 7. Free energy density maps for (a) 90° and (b) 45° Scherk saddles. The maps are projected along the z-axis into the x–y plane. As indicated by the scale bar, the lighter shading corresponds to larger Σ and greater energy per chain. The maps are molecular weight invariant and apply to SB 20/20, 40/40, and 80/80 with the proper calibration of the scale bar.

An analytical formula for the Scherk IMDS† is:

$$\mathbf{S}(u,v) = (x, y, z) = \left(u, v, \frac{1}{\sin\alpha}\ln\left\{\frac{\cos u}{\cos[u\cos\alpha + v\sin\alpha]}\right\}\right) \quad (12)$$

where α is the twist. Using differential geometry,[34] H and K can then be calculated at any point on these surfaces. These calculations are performed in Appendix 5.A of ref 37. Since the Scherk surface is minimal, this calculation yields $H = 0$ and $K \leq 0$ for all points on the IMDS†.

Figure 7 shows free energy density maps for the saddle regions of the 90° (a) and 45° (b) Scherk twist boundaries calculated from eq 10. As indicated by the scale bar, lighter shading represents a higher energy. In the figure the scale bar is calibrated to indicate energy per chain for the three different molecular weights. The maximum energy density occurs in the central regions, near the saddle points, of the 90° and 45° saddles. This maximum energy is the same at the saddle points of all Scherk saddles regardless of the twist angle. It is 10.8, 14.3, and 16.8 kT per chain for SB 20/20, 40/40, and 80/80, respectively. The minimum energy density, which is essentially the flat interface energy, is found at the edges of the maps where the saddles merge into the flat lamellar planes. This minimum energy is 6.8, 9.0, and 11.2 kT per chain for SB 20/20, 40/40, and 80/80, respectively.

The Scherk boundary energy is calculated by integrating the energy per chain given by eq 10 over the Scherk IMDS† given by eq 12. This calculation is carried out as follows:

$$F_{\text{Sch}} = \frac{1}{B}\int\int_{S_u}\frac{F_{\text{tot}}}{\Sigma(K)}\,dA \quad (13)$$

The integral is taken over the IMDS† of a single Scherk unit cell, S_u. The unit cell for the Scherk surface is boldly outlined in Figure 1. This cell is defined such that the entire grain boundary morphology may be constructed by the repeated two-dimensional translation of this basic piece. The total interfacial energy per unit cell is then normalized by the basis, B, for the calculation which may be the unit cell volume, V_u, or by the projected area, of this single cell, in the grain boundary plane, A_u. The ratio F_{tot}/Σ gives the free energy per unit area on the IMDS† as a function of the local K. Here we must use Σ given by eq 8. Due to the complexity of the local evaluation of K on the IMDS†, the integration of eq 13 must be carried out numerically.[52]

The projection of the unit cell of the Scherk surface into the plane of the grain boundary changes from a square into a rhombus as the twist angle, α, is decreased from 90° as shown in GB-I Figure 14. This deformation of the Scherk unit cell occurs in such a way that lamellar thickness is preserved, which causes the rhombus to become very elongated at low twist angles. At zero twist the major diagonal of the rhombus diverges to infinite length. The area of the projection of the Scherk unit cell in the grain boundary plane is given by $A_u = L^2/\sin\alpha$, and the volume per unit cell is $V_u = WA_u$. The determination of W is discussed below. The fact that A_u and V_u diverge as the twist approaches zero is consistent with the transformation of the Scherk boundary into a single screw dislocation as described in GB-I.[1]

The Scherk surface as given by eq 12 includes not only the saddle regions but also the continuous (asymptotic) transition of these saddles into the adjoining planes. Thus there is no precisely defined width of the grain boundary region. A practical definition of the width of the Scherk grain boundary (W), as shown in Figure 1, can be obtained by estimating how far up a saddle one has to go in order to encounter interface that is essentially flat even though mathematically the *model* surface only asymptotically approaches the plane. Many possible criteria could be used to determine the W value at which the interface can be considered *essentially flat*. Here we present results obtained using an energy cutoff criterion which we believe is most physically appropriate for our purpose of calculating grain boundary energies.

In order to determine W, a threshold energy level is chosen and all diblock material with curvature-induced energy greater than this threshold value is considered part of the grain boundary. At some point on the Scherk saddles, as the absolute value of the z-coordinate (Figure 1) increases, the energy falls below the threshold value. This point determines $z_{\text{cutoff}}(x,y)$. Material which is a greater distance from the origin of the z-axis than this cutoff will have a lower energy than the threshold and is thus considered part of the bulk lamellar grains rather than part of the grain boundary. As indicated, the z-coordinate for which the local energy density falls below the cutoff varies with the x and y coordinates on the saddle surface. When integrating energy densities over the Scherk IMDS†, the limits of integration are determined locally by the value of $z_{\text{cutoff}}(x,y)$. Scherk grain boundary width, W, is taken as the sum of the maximum $|z_{\text{cutoff}}|$ values encountered on both sides of the IMDS†. Due to the symmetry of the Scherk saddles, the maximum $|z_{\text{cutoff}}|$ values on both sides of the saddle are equal. Thus $W = 2|z_{\text{cutoff}}|_{\max}$.

The curvature energies encountered in Scherk grain boundaries span the range from a minimum equal to the flat interfacial energy to a maximum at the saddle points where $K = -2.47$. The energy cutoff is then defined as some percentage of this energy range. Material is included in the grain boundary if its energy exceeds the flat interface energy by more than some threshold percentage of the full energy range. Notice that, since curvature-induced energy depends only on K, the energy cutoff criteria could

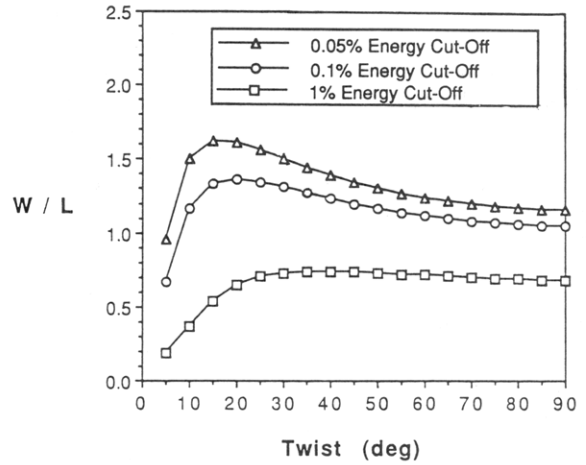

Figure 8. Plots of dimensionless Scherk grain boundary width, W/L, vs twist angle for SB 40/40. The three curves are for energy cutoffs of 1%, 0.1%, and 0.05%.

also be considered a K cutoff criterion. In this study thresholds of 1%, 0.1%, and 0.05% of the full energy range were used in order to study the effects of this cutoff on the results obtained.

Figure 8 plots the dimensionless width, W/L, of the grain boundary region for a Scherk interface vs twist for SB 40/40 as determined by the three different energy cutoffs. Energy cutoff curves for SB 20/20 and 80/80 coincide with those given for SB 40/40 in the figure when the dimensionless representation of boundary width, W/L, is employed. All three energy cutoffs lead to an approximately constant (slightly decreasing with increasing twist) W for twist greater than about 20–30°. For low twist angles, less than 20°, the energy cutoff curves show sharp decreases in W/L as the twist decreases toward zero. The grain boundary width increases with decreasing percentage threshold because we must go further up the sides of the saddle surfaces to find interface where the energy is below a lower cutoff. In the twist range from 20 to 90°, W/L ranges from 0.8 to 0.7 for the 1% energy cutoff, from 1.3 to 1.1 for the 0.1% energy cutoff, and from 1.6 to 1.3 for the 0.05% energy cutoff.

Regardless of the cutoff used, W is approximately 1 or 2 long periods for twists larger than about 20°. The Scherk surfaces shown in the TEM micrographs of GB-I had twists of approximately 80°, 40°, and 30° and indeed displayed grain boundary widths of about a lamellar long period. Examination of the TEM micrograph of a 0° twist Scherk surface (single helicoid screw dislocation) shown in GB-I Figure 17 clearly indicates that the interfacial curvature is concentrated into a narrow boundary region of less than a long period in width. This is in agreement with the energy cutoff results for very low twist angles displayed in Figure 8.

Figure 9 shows histograms of energies per chain in SB 80/80 over Scherk saddle surfaces for three different twist angles: 30°, 60°, and 90°. In constructing these histograms the 0.1% energy cutoff criterion for W determination was used. The total possible range of SB 80/80 energy per chain on the Scherk saddles, 11.2 to 16.8 kT, was divided into 20 equal subranges. The percentage of the entire saddle surface area occupied by chains of a particular energy subrange is plotted vs energy. For all three twist angles the vast majority of the chains fall into the lowest energy subrange. However, as twist increases the proportion of chains with higher energy also increases. The 90° saddle contains the highest percentage of surface area in the higher energy subranges (from 14.0 kT per chain

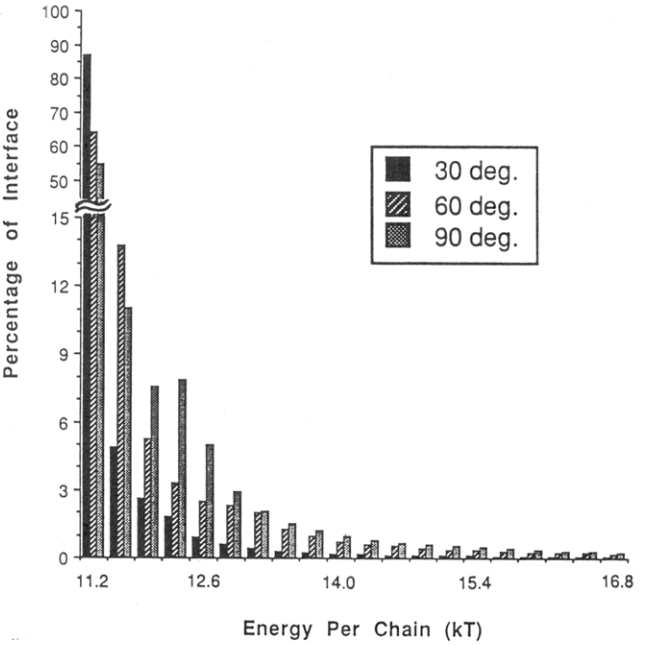

Figure 9. Histogram of chain energies in 30°, 60°, and 90° twist Scherk boundaries. The percentage of total interfacial area occupied by chains falling within each of 20 energy subranges, from 11.2 to 16.8 kT per chain, is plotted vs energy. For all three twist angles the vast majority of the chains fall into the lowest energy subrange. However, as twist increases the proportion of chains with higher energy also increases.

upward); the 60° saddle contains the second most area in the higher energy subranges, and the 30° saddle contains the least. These histogram results are consistent with the energy density maps shown in Figure 7. The lower twist saddles contain much more nearly flat, low-energy IMDS† area than the higher twist angle saddles. Histograms for SB 20/20 and 40/40 display the same relative distribution of chain energies as for SB 80/80, but the energy range is different.

On the basis of these histograms we would expect that an energy per chain averaged over the whole Scherk surface morphology would increase with increasing twist. Energies per chain are calculated by multiplying an average grain boundary energy per unit volume, obtained from eq 13, by V_{pc}. Figure 10a shows the average energy per chain vs twist for SB 80/80. Three results obtained by using the three different energy cutoff criteria for W determination are shown. The average energy per chain shows a sigmoidal curve increasing with increasing twist. Choosing a higher percentage energy cutoff excludes more low curvature interface and thus gives higher weight in the average to the more strongly curved interface nearer to the saddle point. Therefore, the average energy per chain curves is shifted to higher energy as the cutoff threshold is increased. In this study we will mainly utilize results obtained with the 0.1% energy cutoff. Figure 10b compares the variation of the average energies per chain (0.1% energy cutoff) for SB 20/20, 40/40, and 80/80 with twist. The curves with open symbols are the SsSCF results; the curves with the filled symbols were calculated with the WS approach discussed in the next section. All three SsSCF curves display the same sigmoidal increase in average energy with increasing twist. The average energy per chain on the Scherk interface (at a fixed twist angle) scales as $N^{0.35}$, the same as the $F_{tot}(K)$ scaling rule given in eq 11c.

Average energies per chain, as plotted in Figure 10, will be the grain boundary energy measurement of choice for comparing the energy of the Scherk morphology with the

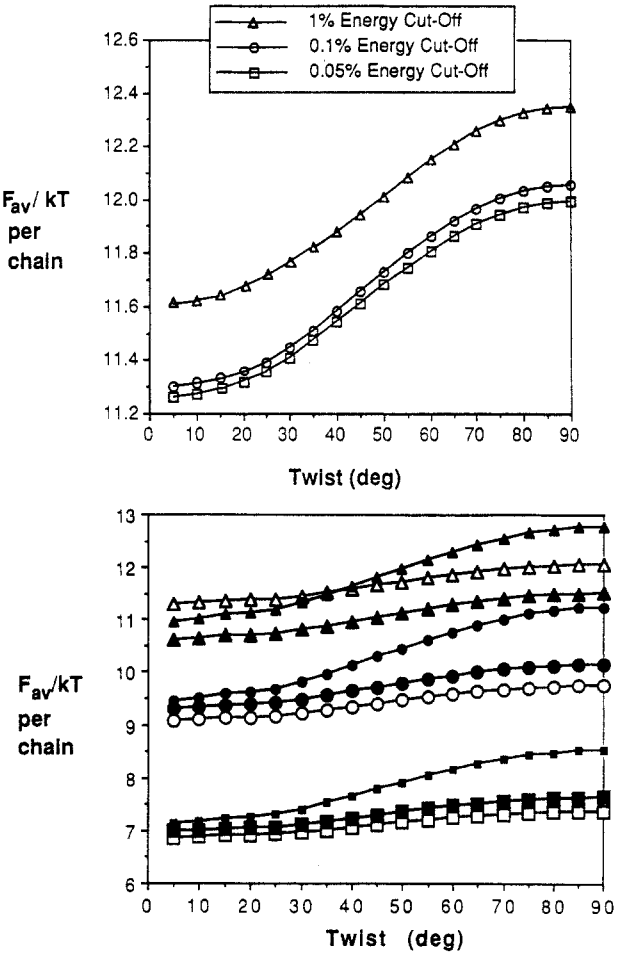

Figure 10. Average energy per chain, F_{av}, vs twist for Scherk grain boundaries. (a) For SB 80/80 three different percentage cutoff criteria were used to determine the grain boundary width, W. The higher the percentage cutoff used, the higher the average energy per chain because a less low-energy, nearly flat interface is included in the calculation. Regardless of the cutoff chosen, F_{av} shows a sigmoidal increase with increasing twist. (b) Average energy per chain vs twist in SB 20/20 (squares), 40/40 (circles), and 80/80 (triangles). The curves with open symbols were calculated using the Scherk specific SCF model; the curves with large filled symbols were calculated using the general WS model with variable Σ; and the curves with the small filled symbols were calculated using the WS model with constant $\Sigma = \Sigma^*$. All three molecular weights and all three calculation models lead to curves that show a sigmoidal increase in the average energy with increasing twist.

energy of the helicoid section grain boundary in GB-III. However, other measures of grain boundary energy are possible, for instance, energy per unit area of the grain boundary plane. The energy per unit grain boundary area is not nearly as useful as the average energy per chain because the energy per area is not an intensive property. As was shown in Figure 8, the width of the grain boundary region varies as a function of twist. Thus the amount of diblock material contributing its energy to a given unit of area in the grain boundary plane changes as a function of twist. These effects are discussed in ref 37.

V. Continuum Theory Calculation Based on the Wang and Safran Model

As mentioned in section III, WS[16-18] employ a power series expansion up to second-order in curvature based on the SCF model of Milner, Witten, and Cates.[35] However, the WS results are strictly applicable only to an isolated diblock layer with relatively small curvature. Such a layer has an imposed curvature but is free of external constraints that may result from interactions with neighboring layers. The Scherk boundary morphology is subject to additional geometric constraints that lead to deviations from the WS results. The deviation of the actual Σ value from the WS Σ on Scherk saddle surfaces was already discussed in section III. We now extend the comparison by calculating Scherk grain boundary energies with the WS method and comparing them with the SsSCF results of the previous section. Obviously since the SsSCF model resulted in the inclusion of a second-order dependence on K, it is a more accurate result which is applicable to higher curvatures. However, it is useful to compare the WS to the SsSCF results in order to determine the limits of applicability of the simpler WS model. The utilization of eq 1 and the WS theory also lead us to examine the application of aspects of differential geometry such as the Gauss–Bonnet theorem and the Gauss normal map to block copolymers.

WS calculate the splay and saddle-splay moduli, k and $\bar{k}$, for eq 1 by setting their curvature free energy expansion equal to eq 1 for the cases of a cylinder and a sphere. This approach was first used for calculating the bending moduli of grafted homopolymer layers by Milner and Witten.[45] The cylinder is a surface of known, constant mean curvature and zero Gaussian curvature. Thus the SCF result for the cylinder can be used to directly determine k.

Then the result of the curvature expansion for the sphere is set equal to eq 1. The value of k is known from the solution for the cylinder so the equation may be solved to give $\bar{k}$.

In this study a simplified version of the WS theory is used in which chain parameters are taken as the same in both blocks. As for the SsSCF work in the previous section, arithmetic averages of PS and PB parameters were used. More involved formulations of this theory are available in which asymmetry in chain statistics is accounted for. However, we are mainly interested in observing qualitative trends in the grain boundary energy calculations and thus will avoid the added computational complexity. WS give the following results for k and $\bar{k}$:

$$k = (3/16)(1 + 3\epsilon^2)(12/\pi^2)^{1/3}N^{5/3}\gamma^{4/3}\nu^{2/3}a^{2/3} \quad (14a)$$

$$\bar{k} = -(1/20)(1 + 12\epsilon^2)(12/\pi^2)^{1/3}N^{5/3}\gamma^{4/3}\nu^{2/3}a^{2/3} \quad (14b)$$

Here ϵ is an asymmetry parameter defined as $1/2 - N_A/N$ which is approximately zero for our nearly symmetric diblocks. γ is interfacial energy or tension which has units of length^{-2} because the energy is normalized by kT. ν is the segmental volume, and a is the segment length.

This solution for k and $\bar{k}$, based on a sphere and cylinder, yields a negative value for $\bar{k}$. This tends to disfavor saddle-shaped bending of the diblock interfaces but would seem to favor deformations that give a positive K. However, as with the area per chain relationship given in eq 2, the mean curvature energy penalty is always positive and outweighs the negative Gaussian curvature term for surfaces of positive K such as spheres.

Working through the units for eq 14, we find that both moduli have units of length^2. When used in eq 1, the length units of these moduli cancel with the curvatures H^2 and K, both of which have units of length^{-2}. This yields a dimensionless value for $f - f_0$ when we wish to calculate an energy/area. The lack of energy units is simply due to normalization by kT and is not a cause for concern. The lack of the length^{-2} units results from the fact that WS prefer to work in terms of energy per chain, and their moduli are calculated to yield $f - f_0$ values on that basis.

We, however, require an energy per unit area to integrate over our geometrical models for the IMDS†. The energy per unit area is found by taking WS's eq 1, on a per chain basis, and dividing through by Σ given by eq 2. This procedure produces dimensionless moduli which may be obtained by dividing the expressions in eq 14 by Σ.

Dividing by Σ, however, creates the difficulty that f_0 and the curvature moduli are no longer constants but are now functions of the interfacial curvature. Therefore, when eq 1 is integrated over an IMDS† with variable curvature, f_0 and the moduli must be continuously reevaluated over the surface. This is particularly undesirable for the case of Gaussian curvature where a mathematical result known as the Gauss–Bonnet theorem (to be discussed below) greatly simplifies the evaluation of the integral of K over the IMDS† but cannot be rigorously applied if $\bar{k}$ is not constant.

The WS calculations were therefore performed in two different ways. (1) The free energy density, calculated with variable f_0 and $\bar{k}$, was numerically integrated over the IMDS†. These results were then compared to the results obtained by the second method. (2) Assume constant f_0 and $\bar{k}$ and utilize the Gauss–Bonnet theorem. The assumption that f_0 and $\bar{k}$ are constant implies that the area per chain is also constant on the IMDS†. For method 2 calculations we assume that the area per chain may be taken equal to the flat interface area per chain, Σ^*. Dividing eq 14b by Σ^* gives the following dimensionless expression for $\bar{k}^*$ which when used in eq 1 gives an energy per unit area suitable for integrating over the IMDS†:

$$\bar{k}^* = -(1/20)(1 + 12\epsilon^2)(12/\pi^2)^{2/3}N^{4/3}\gamma^{5/3}\nu^{2/3}a^{4/3} \tag{15}$$

The scaling of the saddle-splay modulus with N and γ in eq 15 now agrees with that reported by Ajdari and Leibler,[53] who also work on an energy per unit area basis. Their result differs slightly from eq 15 because they were working with a somewhat different system, diblock bilayers.

Using eqs 14b and 15, we find the values of the saddle-splay modulus which are used to calculate twist boundary energies in this study. The values of a, ν, and γ are the same as reported in section IV. The results of these calculations for the three different molecular weights are listed in Table 1. f_0 per chain is given[16] by $(3/2)\gamma\Sigma^*$. Division by Σ^* gives f_0^*, a ground-state energy on a per unit area basis under the assumption that Σ remains constant and equal to Σ^* everywhere on the Scherk saddle. Values of f_0 and f_0^* applicable at the annealing temperature of 120 °C are given in Table 1.

In Table 1, $\bar{k}$ is given in dimensions of $(h^*)^2$ so as to yield energies per chain when multiplied by K which employs length units normalized by the equilibrium brush height, $h^* = L/4$. We can now compare energies per chain as a function of K calculated with the SsSCF model of the previous section and the WS model. Equation 10 gives the SsSCF energies per chain, while eq 1 with f_0 and $\bar{k}$ values from Table 1 gives the WS energies per chain. For a flat interface, the energy per chain is slightly higher in the SsSCF results than in WS for SB 80/80 11.2 kT vs 10.5 kT. In SB 20/20 and 40/40 the SsSCF flat interface energies per chain are slightly lower than the WS values. The linear increase in energy per chain with $|K|$ is found to be considerably stronger with WS than SsSCF. However, the presence of the third term, which is second order in $|K|$ or fourth order in the principal curvatures, augments the increase in energy with $|K|$ for the SsSCF model. Figure 6b gives a comparison of the SsSCF and WS dependencies of energy per chain on $|K|$ for the three diblocks considered. Over the range from 0 to the highest $|K|$ encountered in the Scherk boundaries, 2.47, the SsSCF and WS models yield quite similar results for all three molecular weights.

Recall from section III that for $|K| > 0.506$ the WS model becomes unphysical since there is insufficient space available near the curved interface to contain the entire polymer chain. However, Figure 6b indicates that if this difficulty is ignored we get seemingly realistic results using WS with large $|K|$. The reason for this is as follows: WS underestimate Σ (and thus interfacial energy) for high $|K|$ in the Scherk geometry, which then leads (through conservation of volume) to an overestimate of the chain stretching penalty. These errors off-set one another, leading to energies that are quite similar to the SsSCF results.

In order to calculate Scherk grain boundary energies, eq 1 was integrated over the interface for a unit cell of the grain boundary structure:

$$\frac{F}{kTB} = \frac{1}{B}\left\{\int_{S_u}\frac{f_0}{\Sigma(K)}\,dA + \int_{S_u}\frac{\bar{k}}{\Sigma(K)}K\,dA\right\} \tag{16a}$$

$$\frac{F}{kTB} \approx \frac{1}{B}\left\{f_0^*\int_{S_u}dA + \bar{k}^*\int_{S_u}K\,dA\right\} \tag{16b}$$

In eq 16a, the notation $\Sigma(K)$ indicates that area per chain is a function of Gaussian curvature. Equation 16a is the general application of the WS theory, while eq 16b employs the assumption of Σ everywhere equal to Σ^*, independent of K. Here, as in section IV, S_u is the IMDS† of a single unit cell, and B is the basis for the calculation.

The integral of K over a surface, as utilized in eq 16b, is defined as the total curvature of the surface. A well-known result of differential geometry, the Gauss–Bonnet theorem,[54,55] states that the total curvature of a surface is invariant for deformations of the surface that do not change genus. The family of Scherk surfaces produced by varying the twist angle, α, are all of the same genus. Thus, to the extent that the assumption of a curvature-independent saddle-splay modulus, $\bar{k}^*$, is valid, the curvature contribution to the free energy of Scherk surface grain boundaries is a constant per unit cell, independent of twist.

We now employ an additional result from differential geometry: that the magnitude of the total curvature of a surface is equal to the area of the Gauss normal map of the surface on a unit sphere.[56,57] For a single Scherk saddle, this mapping procedure yields a total curvature of -2π. As indicated in GB-I Figure 14, the unit cell of the Scherk surface contains two saddles of opposite orientation: When viewed from an arbitrarily chosen side of the surface, one saddle has PS above and PB below while the other has the opposite. This results in a total curvature of -4π for the full Scherk unit cell. This value does not change as the twist of the Scherk surface is varied from 0° to 90°. Additionally, this value of the total curvature is scale invariant. Thus the total curvature is the same for the unit cell of a Scherk surface regardless of the actual dimensions of the saddles, regardless, for instance, of the molecular weight of the diblocks forming the surface.

The Gauss–Bonnet theorem tells us that, to the extent that the constant Σ approximation of eq 16b is true, the integral of the curvature energy over the surface is a constant, $-2\pi\bar{k}$ per saddle regardless of twist. This can be seen to be approximately true by examining the free energy density maps in Figure 7 which were calculated using the more accurate SsSCF approach. While the 45° saddle has obviously increased in size and surface area with respect to the 90° saddle, the total curvature is unchanged. Much

of the added surface area in the 45° saddle is occupied by low-curvature, low-energy interface which is dark in the map.

Numerical integrations of eq 16 were carried out over the Scherk saddles utilizing the 0.1% energy cutoff described in section IV for the determination of W. In eq 16b, the basis for the calculation, B, is V_u and the total curvature is -4π. The calculation of the total curvature formally includes the normal map of the complete Scherk surface including the asymptotic planes. However, the contribution to the total curvature of the essentially flat material beyond our small deviation cutoff is negligible.

Referring back to Figure 10b, the large filled symbols indicate energies per chain, averaged over the Scherk interface, calculated using the WS formulation of eq 16a. The WS approach yields the same sort of sigmoidal increase in average energy with increasing twist as does the SsSCF model. Although the WS and SsSCF curves, for each molecular weight, do not exactly agree, the curves are quite close in energy and approximately parallel, increasing by about the same amount of energy ($\sim 0.5\ kT$) as twist increases from 0° to 90°.

Curves calculated using the constant Σ^* version of the WS theory (eq 16b) are also plotted in Figure 10b using the small filled symbols. This version of the WS theory, which utilizes the Gauss–Bonnet theorem, yields higher average energies per chain than eq 16a. Additionally the increase in the average energy per chain over the twist range from 0° to 90° is about three times as large as that obtained with both eq 16a and the SsSCF theory. These results indicate that while the general implementation of the WS theory using eq 16a leads to relatively close agreement with the SsSCF theory, the constant Σ^* assumption degrades the performance of the WS approach considerably. Nevertheless, the results from eq 16b preserve the basic sigmoidal increase in the average energy per chain as twist increases.

In a qualitative way we can use the approximate result obtained with eq 16b to shed additional light on the dependence of the average energy per chain on twist as shown in Figure 10. In this approximation, the curvature energy per unit cell of the boundary is a constant, $-4\pi\bar{k}$, while V_u increases as twist decreases, diverging as twist approaches zero. Thus a constant curvature energy penalty is distributed over a diverging volume (diverging number of chains) as twist approaches zero. In other words, the curvature energy penalty per saddle in the grain boundary is approximately a constant, but as twist is decreased the saddles become larger, thus spreading this constant energy over a larger amount of material. This leads to a decrease in the average energy per chain as twist is decreased.

WS theory also leads to a slightly different dependence of average energy per chain on molecular weight than the SsSCF model. This is made apparent in Figure 10b by the fact that the WS (eq 16a) curve is above the SsSCF for the lower two molecular weights but below the SsSCF curve for SB 80/80. Substituting scaling relationships for f_0, $\bar{k}$, and K into eq 1, we find that the WS theory predicts that energies per chain should scale as $N^{1/3}$. However, as discussed in section IV the SsSCF calculations yielded the scaling dependence $N^{0.35}$. This slight difference between the WS and SsSCF scaling relationships results from a combination of two effects. First, the actual microdomain dimensions used in the SsSCF calculations were found to scale as $N^{0.69}$, rather than $N^{2/3}$ as assumed by WS. Second, the additional geometric constraints present in the Scherk grain boundary morphology may have altered the scaling.

VI. Conclusions

We have calculated energies per chain and energies per unit grain boundary area for lamella-forming diblock copolymers in the Scherk surface twist boundary morphology. Three different methods of calculation were used. In the SsSCF model, average energies per chain were rigorously calculated for all the possible interfacial curvature environments encountered by diblocks in the Scherk morphology. The Wang and Safran (WS) approach utilized moduli to impose energetic penalities for curvature of the interface in the grain boundary region. The WS theory was implemented in two ways. First, we allowed for a variable area per chain, Σ, on the IMDS† and numerically integrated the expression for free energy density over the interface. Second, we assumed that Σ was unchanged from its flat interface value, Σ^*, by interfacial curvature. Through the application of the Gauss–Bonnet theorem, the integration of the free energy density over the IMDS† was greatly simplified. The WS approach with variable Σ yielded results which agreed quite closely with those found using the SsSCF approach. This was despite the fact that the WS model becomes unphysical for strong curvatures due to the unique geometric constraints of the Scherk boundary morphology. The results of the WS approach with fixed $\Sigma = \Sigma^*$ were not as quantitatively close to the SsSCF results; however, they were still qualitatively quite good. In addition the Gauss–Bonnet theorem, in this simplified formulation, allows a clearer understanding of the trend of decreasing average energy per chain with decreasing twist found with all three calculational methods. Thus, of all the Scherk family defect structures observed in GB-I the zero degree twist, single screw dislocation (GB-I Figures 16 and 17) is believed to be the most stable.

We will continue our study of lamellar diblock copolymer twist grain boundary morphology in GB-III. Here we will calculate grain boundary energies for the helicoid section morphology and make comparisons between helicoid section and Scherk boundary energies as a function of twist.

Acknowledgment. We thank Dr. L. J. Fetters of Exxon for synthesizing the diblock copolymers and Profs. H. Karcher, D. Hoffman, R. Kusner, and P. Smith for discussions on differential geometry. Computer graphics of minimal surfaces were generated at GANG (the Center for Geometry, Analysis, Numerics, and Graphics) at the University of Massachusetts, Amherst, with the help of J. T. Hoffman. We thank Dr. R. Lescanec for helpful discussions of grafted chain theory and for aiding in revisions to the manuscript. S.P.G. thanks the organizers of the 1991 NSF Summer Research Institute on Graphics and Computation in Differential Geometry at which many difficulties in this research were resolved. Funding was provided by NSF-DMR 8907433, AFOSR 910078, and CMSE 9022933.

References and Notes

(1) Gido, S. P.; Gunther, J.; Thomas, E. L.; Hoffman, D. *Macromolecules* **1993**, *26*, 2636.
(2) Gido, S. P.; Thomas, E. L., in preparation.
(3) Scherk, H. F. *J. Reine Angew. Mat.* **1835**, *13*, 185.
(4) Helfand, E. *Acc. Chem. Res.* **1975**, *8*, 297.
(5) Helfand, E.; Wasserman, Z. R. *Macromolecules* **1976**, *9*, 879.
(6) Helfand, E.; Wasserman, Z. R. *Polym. Eng. Sci.* **1977**, *17*, 582.
(7) Helfand, E.; Wasserman, Z. R. *Macromolecules* **1978**, *11*, 960.
(8) Helfand, E.; Wasserman, Z. R. *Macromolecules* **1980**, *13*, 994.
(9) Ohta, T.; Kawasaki, K. *Macromolecules* **1986**, *19*, 2621.

(10) Semenov, A. N. *Sov. Phys. JETP* **1985**, *61*, 733.
(11) Birshtein, T. M.; Zhulina, E. B. *Polymer* **1990**, *31*, 2197.
(12) Birshtein, T. M.; Zhulina, E. B. *Polymer* **1990**, *31*, 1312.
(13) Fredrickson, G. H. *Macromolecules* **1991**, *24*, 3456.
(14) Olvera de la Cruz, M. *Phys. Rev. Lett.* **1991**, *67*, 85.
(15) Olvera de la Cruz, M.; Mayes, A. M.; Swift, B. W. *Macromolecules* **1992**, *25*, 944.
(16) Wang, Z.-G.; Safran, S. A. *J. Phys. (Paris)* **1990**, *51*, 185.
(17) Wang, Z.-G.; Safran, S. A. *Europhys. Lett.* **1990**, *11*, 425.
(18) Wang, Z.-G.; Safran, S. A. *J. Chem. Phys.* **1991**, *94*, 679.
(19) Fredrickson, G. H.; Binder, K. *J. Chem. Phys.* **1989**, *91*, 7265.
(20) Smith, C. S. *Metallurg. Rev.* **1964**, *9*, 1.
(21) Voronoï, G. *J. Reine Angew. Mat.* **1908**, *134*, 198.
(22) Medvedev, N. N. *J. Comput. Phys.* **1986**, *67*, 223.
(23) Fredrickson, G. H., personal communication.
(24) Bouligand, Y. *J. Phys. (Paris)* **1972**, *33*, 525.
(25) de Gennes, P.-G. *The Physics of Liqid Crystals*; Oxford University Press: New York, 1974.
(26) Kléman, M. *Points, Lines, and Walls*; John Wiley and Sons: New York, 1983.
(27) Orowan, E. *Nature* **1942**, *149*, 643.
(28) Argon, A. S. In *Treatise of Materials Science and Technology*; Academic Press: New York, 1972; Vol. 1.
(29) Evans, A. G.; Adler, W. F. *Acta Metallurg.* **1978**, *26*, 725.
(30) Martin, D. C. Ph.D. Thesis, University of Massachusetts, Amherst, MA, 1989.
(31) Vezie, D. L. Personal communication.
(32) Robertson, R. E. *J. Polym. Sci., Polym. Phys. Ed.* **1969**, *1*, 1315.
(33) de Teresa, S. J.; Porter, R. S.; Farris, R. J. *J. Mater. Sci.* **1988**, *23*, 1886.
(34) Struik, D. J. *Lectures on Classical Differential Geometry*, 2nd ed.; Dover: New York, 1961; pp 61 and 62.
(35) Milner, S. T.; Witten, T. A.; Cates, M. E. *Macromolecules* **1988**, *21*, 2610.
(36) Zhulina, E. B.; Liatskaya, Y. V.; Birshtein, T. M. *Polymer* **1992**, *33*, 332.
(37) Gido, S. P. Ph.D. Thesis, Chemical Engineering, Massachusetts Institute of Technology, 1993.
(38) Frank, F. C. *Discuss. Faraday Soc.* **1958**, *25*, 19.
(39) Leibler, S. In *Statistical Mechanics of Membranes and Surfaces*; Nelson, D., Piran, T., Weinberg, S., Eds.; World Scientific: Singapore, 1989; Vol. 5; pp 46–103.
(40) Huse, D. A.; Leibler, S. *J. Phys. (Paris)* **1988**, *49*, 605.
(41) Helfrich, W. *Z. Naturforsch.* **1973**, *28*, 693.
(42) Kléman, M. *Proc. R. Soc. London* **1976**, *347*, 387.
(43) Kléman, M.; Parodi, O. *J. Phys. (Paris)* **1975**, *36*, 671.
(44) de Gennes, P.-G. *J. Phys. (Paris)* **1969**, *30*, C4–65.
(45) Milner, S. T.; Witten, T. A. *J. Phys. (Paris)* **1988**, *49*, 1951.
(46) Milner, S. T. *Science* **1991**, *251*, 905.
(47) Helfand, E.; Tagami, Y. *J. Chem. Phys.* **1972**, *56*, 3592.
(48) Mori, K.; Hasagawa, H.; Hashimoto, T. *Polym. J.* **1985**, *17*, 799.
(49) Alexander, S. *J. Phys. (Paris)* **1977**, *38*, 977.
(50) de Gennes, P.-G. *J. Phys. (Paris)* **1976**, *37*, 1443.
(51) de Gennes, P.-G. *Macromolecules* **1980**, *13*, 1069.
(52) Grain boundary energy calculations are done with energy normalized by kT and length measured in dimensionless "mathematical units". Mathematical units, abbreviated "mu", are defined such that one long period of the lamellar structure is equal to 2π mu. Thus mu's are larger for higher molecular weight diblocks. The dimensionless mu length unit is necessary when using eq 12 to describe the Scherk grain boundary model. Lamellar long periods, L, for the three diblocks used in this study were determined by small-angle X-ray scattering (SAXS) in order to obtain the following relationships between physical and mathematical length units for each polymer: $L(20/20) = 387$ Å $= 2\pi mu_{20/20}$; $L(40/40) = 625$ Å $= 2\pi mu_{40/40}$; $L(80/80) = 1060$ Å $= 2\pi mu_{80/80}$.
(53) Ajdari, A.; Leibler, L. *Macromolecules* **1991**, *24*, 6803.
(54) Hoffman, D. A. *J. Phys., Colloq.* **1990**, *51*, C7–197.
(55) David, F. In *Statistical Mechanics of Membranes and Surfaces*; Nelson, D., Piran, T., Weinberg, S., Eds.; World Scientific: Singapore, 1989; Vol. 5, p 157.
(56) Hsu, L.; Kusner, R.; Sullivan, J. GANG Preprint Series III.1, 1992.
(57) Hilbert, D.; Cohn-Vossen, S. *Geometry and the Imagination*; Chelsea: New York, 1952.
(58) Ball, R. C.; Marko, J. F.; Milner, S. T.; Witten, T. A. *Macromolecules* **1991**, *24*, 679.
(59) Melenkevitz, J.; Muthukumar, M. *Macromolecules* **1991**, *24*, 4199.
(60) Gido, S. P.; Lescanec, R. L.; Thomas, E. L. *Macromolecules*, in preparation.